

# Fatigue mechanism verified using photovoltaic properties of $\text{Pb}(\text{Zr}_{0.52}\text{Ti}_{0.48})\text{O}_3$ thin films

Cite as: Appl. Phys. Lett. **110**, 133903 (2017); <https://doi.org/10.1063/1.4979525>

Submitted: 22 December 2016 . Accepted: 18 March 2017 . Published Online: 30 March 2017

Ming Wu, Wei Li, Junning Li, Shaolan Wang, Yaqi Li, Biaolin Peng, Haitao Huang , and Xiaojie Lou



View Online



Export Citation



CrossMark

## ARTICLES YOU MAY BE INTERESTED IN

[Polarization-dependent photovoltaic effect in ferroelectric-semiconductor system](#)

Applied Physics Letters **110**, 121105 (2017); <https://doi.org/10.1063/1.4978749>

[Photovoltaic and photo-capacitance effects in ferroelectric  \$\text{BiFeO}\_3\$  thin film](#)

Applied Physics Letters **110**, 192906 (2017); <https://doi.org/10.1063/1.4983378>

[Ferroelectric, pyroelectric, and piezoelectric properties of a photovoltaic perovskite oxide](#)

Applied Physics Letters **110**, 063903 (2017); <https://doi.org/10.1063/1.4974735>

Lock-in Amplifiers  
Find out more today



Zurich  
Instruments

## Fatigue mechanism verified using photovoltaic properties of $\text{Pb}(\text{Zr}_{0.52}\text{Ti}_{0.48})\text{O}_3$ thin films

Ming Wu,<sup>1</sup> Wei Li,<sup>1</sup> Junning Li,<sup>1</sup> Shaolan Wang,<sup>1</sup> Yaqi Li,<sup>1</sup> Biaolin Peng,<sup>2,3</sup> Haitao Huang,<sup>3</sup> and Xiaojie Lou<sup>1,a)</sup>

<sup>1</sup>Frontier Institute of Science and Technology, and State Key Laboratory for Mechanical Behavior of Materials, Xi'an Jiaotong University, Xi'an 710049, People's Republic of China

<sup>2</sup>School of Physical Science and Technology and Guangxi Key Laboratory for Relativistic Astrophysics, Guangxi University, Nanning 530004, People's Republic of China

<sup>3</sup>Department of Applied Physics, The Hong Kong Polytechnic University, Kowloon, Hong Kong

(Received 22 December 2016; accepted 18 March 2017; published online 30 March 2017)

The photovoltaic effect and its evolution during electrical fatigue in  $\text{Pb}(\text{Zr}_{0.52}\text{Ti}_{0.48})\text{O}_3$  (PZT) thin films have been investigated. It is found that the photovoltaic effect of the as-grown PZT thin film is highly affected by the asymmetric Schottky barriers, which can be tuned by applying an external electric field. During fatigue processes, both open-circuit voltage ( $V_{oc}$ ) and short-circuit current ( $J_{sc}$ ) decrease considerably with the increase of the number of electrical cycles. This phenomenon could be ascribed to the degradation of the interfacial layer between the thin film and the electrode induced by highly energetic charge carriers injected from the electrode during bipolar cycling. Our work sheds light on the physical mechanism of both ferroelectric photovoltaics and polarization fatigue in thin-film ferroelectrics. *Published by AIP Publishing.*

[<http://dx.doi.org/10.1063/1.4979525>]

Ferroelectric materials have spontaneous electric polarization ( $P_s$ ) below a certain temperature  $T_c$  (the Curie temperature), and their polarization can be reversibly switched by applying an external electric field.<sup>1</sup> Thanks to these useful properties, ferroelectric materials have been widely used in a variety of device applications, such as photovoltaic devices<sup>2-5</sup> and ferroelectric random access memories (FeRAMs). The basic working principle of FeRAMs is that the up and down states of the spontaneous polarization of ferroelectrics could be coded as the “1” and “0” states, respectively. FeRAMs have many advantages over other memory devices, such as non-volatility, radiation hardness, and faster reading/writing speed.<sup>6</sup> However, FeRAMs generally suffer from severe polarization fatigue during the information reading and writing processes.<sup>6</sup> The phenomenon of polarization fatigue in ferroelectrics has been intensively investigated for many years, and a number of models and mechanisms have been proposed in the literature, including the domain pinning model,<sup>7,8</sup> the interface nucleation inhibition mechanism,<sup>9</sup> mechanical destruction,<sup>10</sup> the formation of a “dead or blocking layer,”<sup>11</sup> and the LPD-SICI model (LPD-SICI stands for local phase decomposition caused by switching induced charge injection). In particular, the LPD-SICI model developed in our previous work<sup>12,13</sup> could interpret the formation of the dead layer during fatigue and is also in good agreement with many of the experimental observations published previously.<sup>14-17</sup> However, the questions as to how the dead layer forms during the process of electrical fatigue and what its properties are remain unclear.

On the other hand, ferroelectric photovoltaic devices, which possess reversibly switchable photovoltaic effects<sup>2</sup> and beyond-bandgap open-circuit voltage  $V_{oc}$ ,<sup>3,18</sup> have

attracted much research interest in recent decades. In a ferroelectric photovoltaic device, the photo-generated charge carriers are partially separated by the internal field induced by spontaneous polarization,<sup>19</sup> which is different from the traditional photovoltaic device, where the photo-generated carriers are separated by the electric field induced by the  $p$ - $n$  junction. The recent research result shows that the interfacial contact between the electrode and thin films is very important to the photovoltaic effect,<sup>20</sup> and fatigue could also be partially blamed on the degradation of the interfacial contact.<sup>11</sup> Thus, it is reasonable to believe the relevance between ferroelectric photovoltaic and polarization fatigue. In this work, we report the ferroelectric photovoltaic effect of the  $\text{Pb}(\text{Zr}_{0.52}\text{Ti}_{0.48})\text{O}_3$  thin film and its fatigue characteristics. The change in ferroelectric photovoltaic as a function of fatigue cycles is studied. It is found that both the open-circuit voltage  $V_{oc}$  and the short-circuit current  $J_{sc}$  are highly sensitive to the number of fatigue cycles.

$\text{Pb}(\text{Zr}_{0.52}\text{Ti}_{0.48})\text{O}_3$  thin films were prepared by using a sol-gel method on Pt(111)/ $\text{TiO}_2$ /SiO<sub>2</sub>/Si(100) substrates, as described in detail elsewhere.<sup>21</sup> The Pt top electrodes of ~30 nm in thickness were sputtered onto the thin film through a square shadow mask with the edge length of 0.42 mm. The structural characteristics of the films were studied by X-ray diffraction (XRD). Scanning electron microscopy (SEM) was performed to examine the film thickness and the cross-section morphology. The photovoltaic  $I$ - $V$  characteristic curves were recorded by using a Keithley 2400 source meter under the standard solar illumination (AM1.5) provided by a Xenon lamp. The leakage currents of the Pt/Pb( $\text{Zr}_{0.52}\text{Ti}_{0.48}$ )O<sub>3</sub> (PZT)/Pt thin films were recorded by using a Keithley 6517B electrometer to analyze the Schottky barriers both in the top and bottom film-electrode interfaces. To avoid the contribution from polarization switch current, a

<sup>a)</sup>Email: xlou03@mail.xjtu.edu.cn

test voltage, lower than the coercive voltage, was selected, and it ranges from  $-3$  V to  $3$  V. The hysteresis loop and fatigue measurements were performed by using a precision ferroelectric tester (Radiant Technologies). A square waveform of  $8$  V in amplitude and  $100$  MHz in frequency was used to fatigue the sample.

Fig. 1 shows the XRD pattern of the PZT thin film fabricated on the Pt(111)/TiO<sub>x</sub>/SiO<sub>2</sub>/Si(100) substrate. It shows that the film is polycrystalline with a pure perovskite phase. No secondary phases can be identified. The film has a smooth surface with a homogeneous thickness of  $\sim 254$  nm, as shown in the inset of Fig. 1.

Fig. 2 displays the current density-voltage ( $I$ - $V$ ) curves under four different poling states, that is, the as-grown state, the Pr-UP state, the Pr-DOWN state, and the dark state. The As-grown PZT thin film shows an open circuit voltage ( $V_{oc}$ ) of  $-0.7$  V and a short circuit current ( $J_{sc}$ ) of  $2 \mu\text{A}/\text{cm}^2$ . The top electrodes are defined as the anodes, which is different from those reported previously.<sup>22</sup> In our case, a negative  $V_{oc}$  and a positive  $J_{sc}$  could be obtained. In order to reveal the relationship between the photovoltaic effect and the ferroelectricity of the PZT thin films, a  $10$  V (or  $-10$  V) voltage was used to pole the thin films, and the tested  $I$ - $V$  curves are shown in Fig. 2. Compared with the as-grown state,  $J_{sc}$  increases from  $2$  to  $4 \mu\text{A}/\text{cm}^2$  in the Pr-up state, while it decreases from  $2$  to  $1.8 \mu\text{A}/\text{cm}^2$  in the Pr-down state. The photovoltaic effect could be characterized by not only the  $I$ - $V$  curves but also the quantum efficiency, as reported in the PZT<sup>22-24</sup> and BFO<sup>25,26</sup> thin films. Normally, the quantum efficiency of PZT thin films peaked at around  $340$  nm, corresponding to the band gap of the PZT thin films ( $3.6$  eV (Ref. 22)).

The semi-log plots of the temperature dependent current density-voltage ( $J$ - $V$ ) curves are shown in Figs. 3(a) and 3(b). Generally, the leakage current of a ferroelectric capacitor with a typical MFM structure depends on the two following points: the thin film itself and the interface between the electrode and the film.<sup>1</sup> Since the same capacitor was used, the difference between the negative and positive branches of leakage current is caused by different Schottky barriers at the film interfaces, whose conduction obeys the Schottky emission mechanism.<sup>20</sup> When a positive voltage is applied

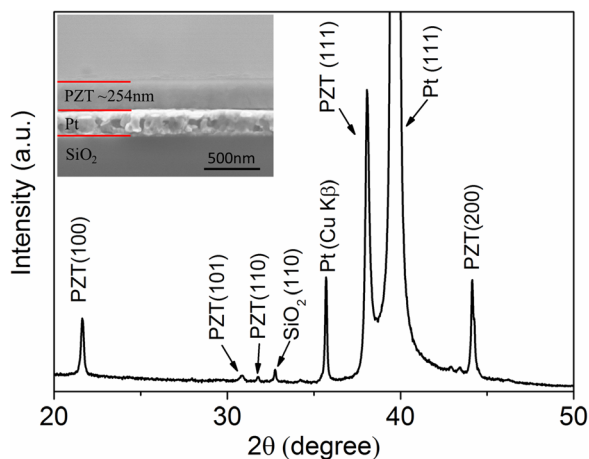


FIG. 1. XRD pattern of the Pb(Zr<sub>0.52</sub>Ti<sub>0.48</sub>)O<sub>3</sub> thin film fabricated on a Pt(111)/TiO<sub>x</sub>/SiO<sub>2</sub>/Si(100) substrate. Inset: the cross-sectional SEM image.

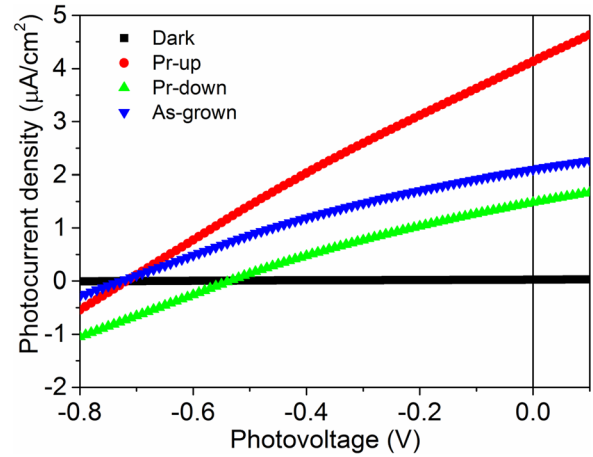


FIG. 2. Dependence of the photovoltaic effect on the polarization direction.

on the top electrode, the electrical field points downward, parallel with  $E_{bi-bottom}$  but antiparallel with  $E_{bi-top}$ . Therefore, the positive branch of leakage is determined by the bottom Schottky barrier, while the negative one is determined by the top Schottky barrier. Both of these two leakage curves could be fitted using the Schottky emission mechanism<sup>27,28</sup>

$$J = A^{**} T^2 \exp \left[ \frac{-q \left( \Phi_B - \sqrt{\frac{qV}{4\pi\epsilon\epsilon_0 w}} \right)}{kT} \right], \quad (1)$$

where  $J$  is the current density,  $A^{**}$  the effective Richardson's constant,  $q$  the charge of an electron,  $\Phi_B$  the Schottky barrier,  $V$  the applied voltage,  $\epsilon$  the dielectric constant,  $\epsilon_0$  the vacuum dielectric constant, and  $k$  the Boltzmann constant. Based on this, the Schottky barrier heights are concluded following the processes described elsewhere.<sup>20,23,29</sup> In the Pr-up state, the Schottky barrier heights at the bottom Pt/PZT interface and at the top PZT/Pt interface are  $0.79$  eV and  $0.49$  eV, respectively, while in the Pr-down state, these Schottky barrier heights are  $0.73$  eV and  $0.58$  eV. The schematics of the energy band diagram with the quantified Schottky barriers in different poling states are shown in Figs. 3(c) and 3(d).

First, we find that in both Pr-up and Pr-down states, the Schottky barrier heights  $\Phi_{bottom}$  are larger than  $\Phi_{top}$ . The asymmetric back-to-back Schottky barriers might be the reason for the photovoltaic effect in the as-grown state. In ferroelectric photovoltaic devices, the internal electrical field separating the photo-generated carriers originates from the combination of ferroelectric spontaneous polarization,<sup>29,30</sup> the depolarization field,<sup>31</sup> and the Schottky barriers in the top and bottom interfaces.<sup>30</sup> Since the as-grown state mainly consists of domains with randomly orientated polarization, its photovoltaic response is believed to be mainly originated from the Schottky barriers in our case. Since the electron affinity of PZT is about  $2.15$  eV and the work function of Pt is about  $5.3$  eV,<sup>32</sup> a built-in electrical field ( $E_{bi-top}$  and  $E_{bi-bottom}$ ) induced by the back-to-back Schottky barriers is formed in the Pt/PZT/Pt capacitors, as shown in Figs. 3(c) and 3(d). It is known that annealing processes affect the defect redistribution, oxygen vacancy concentration, and PbO volatilization in PZT thin films, especially at the interface.<sup>33</sup> What's more, as reported by Shen *et al.*<sup>20</sup> believe that the loss of PbO at the top interface during the annealing process may form a conductive

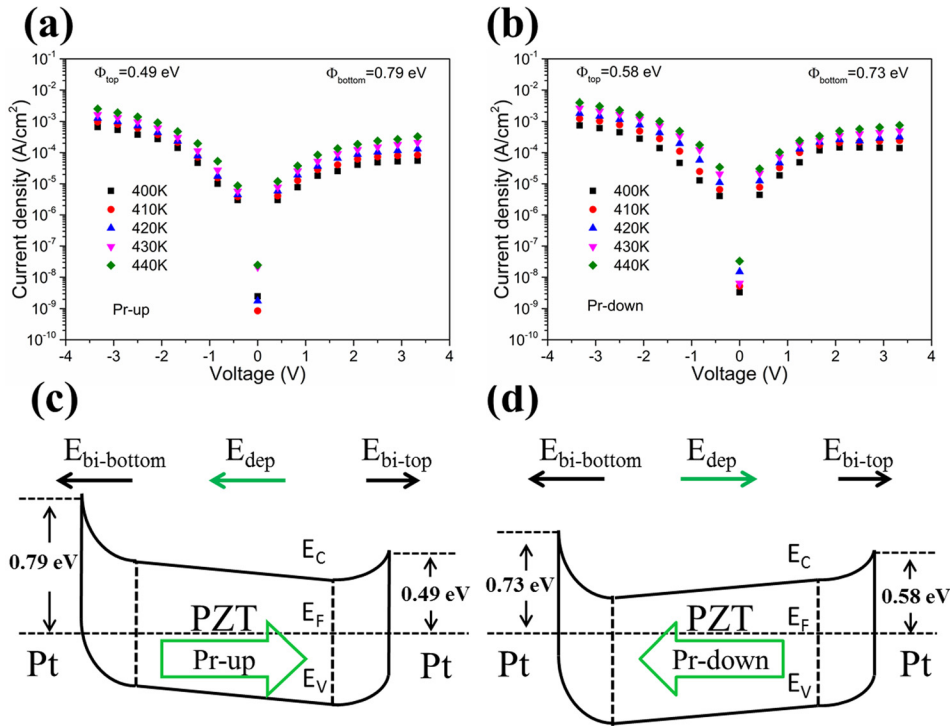


FIG. 3. Temperature dependence of J-V curves in (a) the Pr-up state and (b) the Pr-down state. The schematics of the energy band diagram with quantified Schottky barrier height in (c) the Pr-up state and (d) Pr-down state in the Pt/PZT/Pt capacitor.

layer and lead to a lower barrier at the top Pt/PZT contact. As a result, the total electrical field  $E_{bi}$  ( $E_{bi} = E_{bi-bottom} - E_{bi-top}$ ) induced at the asymmetric Schottky barriers points downward, acting as the internal built field to separate the photo-generated carriers in the as-grown state. What's more, the internal built electrical field and the photovoltaic effect also affected by the space charges in the grain boundaries in the polycrystalline PZT thin films. As reported by Xu *et al.*,<sup>34</sup> they found an abnormal sharp peak of photocurrent within 10s after poling, and they attributed this to time-dependent space charges. During the poling process, the carriers were injected and located on different trap levels, changing the internal field with consequence over the photocurrent. After poling, the trapped carriers are released over time, and the induced internal field and abnormal photocurrent disappeared. In our as-grown state samples, the effect of space charges on the photovoltaic effect was very weak. In the poling state samples, we test the photovoltaic effect after poling for 1 min, carefully avoiding the impact of the abnormal phenomenon.

Then, the  $\Phi_{bottom}$  in the Pr-up state (0.79 eV) is higher than that in Pr the -down state (0.73 eV), and the  $\Phi_{top}$  in the Pr-up state (0.49 eV) is lower than that in the Pr-down state (0.58 eV). The polarization dependence of Schottky barrier heights might be the reason for the polarization dependence of the photovoltaic effect, which could be well explained by the so-called depolarization field ( $E_{dep}$ ) effect mentioned previously. As schematically shown in Fig. 3(c), when the thin film is poled to the up state,  $E_{dep}$  is built, points downward, enhances  $\Phi_{bottom}$ , decreases  $\Phi_{top}$ , and finally enlarges  $E_{bi}$ , leading to the enhanced photovoltaic effect. However, when the thin film is poled to the down state, as shown in Fig. 3(d), the results are converse.

The bipolar electrical fatigue properties of the film, the polarization-voltage hysteresis loops, and the photovoltaic responses in different fatigue states are shown in Fig. 4. In

Fig. 4(a), we can see that the film shows a typical fatigue degradation curve with an increasing number of electrical cycles. It consists of three different stages: the slow fatigue stage (from point A to C), the logarithmic stage (from point C to around  $10^8$  cycles), and the saturated stage (from around  $10^8$  cycles to point D), which is consistent with the work published previously.<sup>16</sup> We chose four points (A, the virgin film; B, that after  $10^5$  cycles; C, that after  $10^7$  cycles; and D, that after  $10^9$  cycles; as shown in Fig. 4(a) to study the evolution of polarization fatigue, and the corresponding  $P$ - $V$  loops and the photovoltaic responses associated. The results are shown in Figs. 4(b)–4(d). From points A to B, the spontaneous polarization shows little change.  $V_{oc}$  keeps almost constant, and  $J_{sc}$  increases a little from 3.5 to 3.8  $\mu\text{A}/\text{cm}^2$ . This is reasonable because initial switching induces the rearrangement of randomly distributed domain walls, which are believed to have better conductivity than the domains and grains.<sup>35–37</sup> The alignment of domain walls forms conducting channels in the film and therefore enhances the collection of the photo-generated carriers. This result is also consistent with our previous studies, where we found that the dielectric constant increased slightly after the initial  $5 \times 10^5$  cycles.<sup>36</sup>

From points B to C and to D, the evolution of spontaneous polarization and the photovoltaic responses during the fatigue processes can be well explained by using the local phase decomposition caused by the switching-induced charge injection<sup>12,13</sup> (LPD-SICI) model. In this model, an extremely high depolarization electric field  $E_{bc}$  may be generated near the electrodes by the bound charges at the tip of the needlelike domains during switching. The local injected power density is given as  $E_{bc}J$ , where  $J$  is the current injected from electrode during switching, producing abundant Joule heating, leading to local phase decomposition at randomly distributed domain nucleation sites.

As demonstrated above, the photovoltaic response in the as-grown PZT thin film is mainly attributed to the

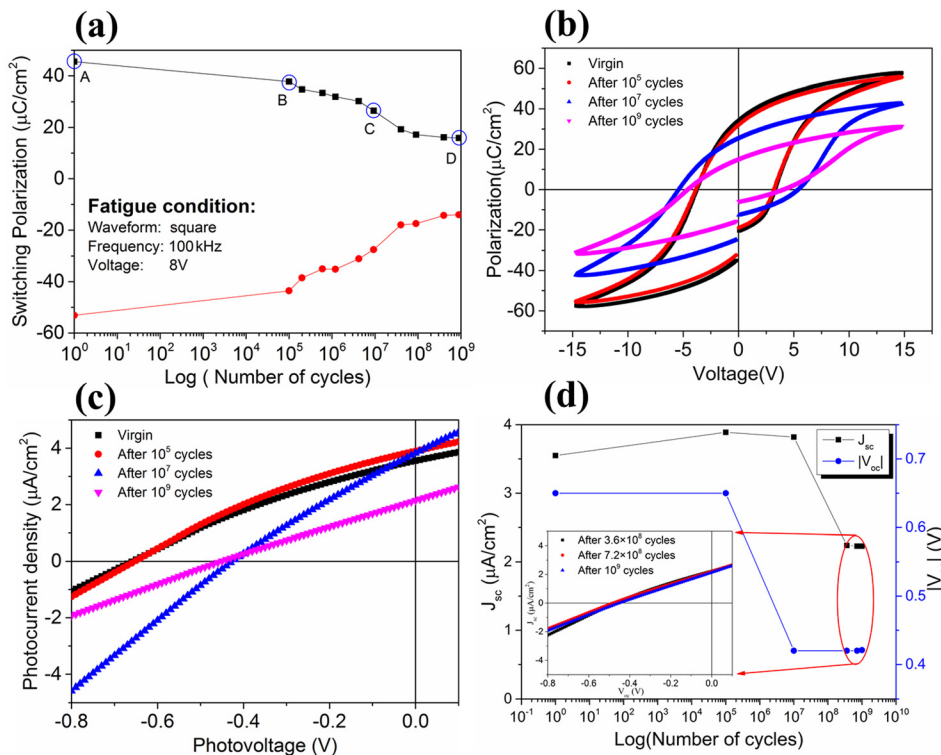


FIG. 4. (a) Fatigue characteristic curves of the PZT thin films. The blue circles A, B, C, and D show the stages selected to test the photovoltaic effect. (b) Polarization-voltage hysteresis loops of the selected four stages and (c) the corresponding photovoltaic effect. (d) The  $J_{sc}$  and  $|V_{oc}|$  as a function of cycles. The inset shows the photovoltaic effects in the saturated fatigue stages.

asymmetric Schottky barriers. This is consistent with the data from points B to C, where  $E_{dep}$  decreases significantly, while  $J_{sc}$  remains constant. Therefore, the evolution of the photovoltaic effect can be ascribed to the change in the Schottky contact in the interface induced by LDP-SICI during fatigue processes. From points B to C,  $J_{sc}$  remains the same and  $V_{oc}$  decreases from  $-0.65$  V to  $-0.42$  V, as shown in Fig. 4(c). During the fatigue processes, the local phase decomposition occurs at the randomly distributed domain nucleation sites, producing many “dead dots,” as shown schematically in Fig. 5(b). The “dead dots,” which possess a lower dielectric constant than that of the fresh films, change the Schottky contact and consequently  $E_{bi-top}$  and  $E_{bi-bottom}$ , leading to the decrease in  $V_{oc}$ . The reason for the unchanged  $J_{sc}$  in the initial fatigue stage is that the “dead dots” are distributed separately at the interface and do not penetrate through the film, therefore having little influence on the conductivity of the film. From points C to D, as shown in Fig. 4(c),  $J_{sc}$  decreases from  $3.8$  to  $2.1$   $\mu\text{A}/\text{cm}^2$ , while  $V_{oc}$  remains almost stable. As the fatigue process continues, the randomly distributed “dead dots” increase in total number, and they connect to each other to form a continuous “dead interface layer,” as illustrated in Fig. 5(c). The formation of the “dead layer” cuts off the conducting channel and resulted in the complete degradation of the photovoltaic effect. In order to

confirm the formation of the “dead layer,” we checked the photovoltaic effect after  $3.6 \times 10^8$ ,  $7.2 \times 10^8$ , and  $10^9$  cycles, respectively, and the results are shown in the inset of Fig. 4(d). A negligible change in the photovoltaic response at these three different points can be observed, implying the formation of the “dead layer” at the beginning of the saturated fatigue stage.

By referring the LPD-SICI mechanism, we can understand the evolution of the interface during the fatigue processes: (1) In the slow fatigue stage, the reverse domain nucleation sites appear randomly, and there is no or slight fatigue; (2) In the logarithmic fatigue stage, the domain nucleation sites start to phase decompose due to charge injection induced by polarization switching, and the “dead dots” are formed. As the number of fatigue cycles further increases, local phase decomposition takes place continuously at the interface, and the “dead dots” are connected to each other to form the “dead layer.” (3) In the saturated stage, the “dead layer” is formed completely, and its thickness increases slowly with the increase of the cycle number. The poor conductivity of the “dead layer” reduces the field seen by the bulk film and therefore leads to the abrupt decrease in the fatigue rate.

In summary, the fatigue mechanism of Pt/PZT/Pt ferroelectric thin films has been studied by testing the photovoltaic responses at different fatigue stages. Combined with the

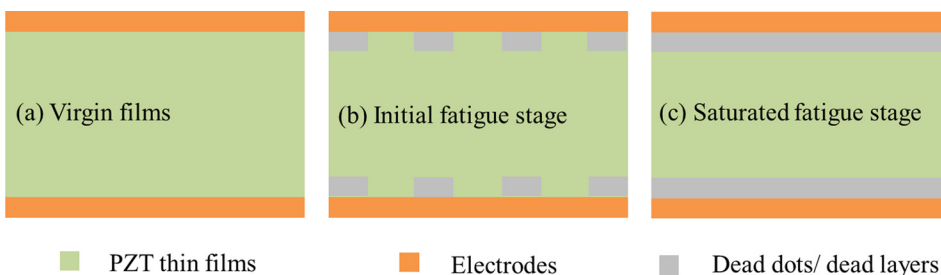


FIG. 5. Schematic mechanism of the capacities under different fatigue stages. (a) The virgin thin films correspond to blue circle A. (b) The initial fatigued thin films correspond to blue circle C. (c) The saturated fatigued thin films correspond to blue circle D.

photovoltaic responses obtained and the LPD-SICI model established by the present authors, we believe that (1) the slow fatigue stage contains pre-formed dead dots; (2) in the logarithmic stage, dead dots are formed and connected; and (3) the dead layer is formed in the saturated fatigue stage. Our results may provide a better understanding of the mechanism of ferroelectric photovoltaic and the microstructural evolution in the Pt/PZT/Pt interfaces during fatigue processes.

This work was supported by the National Science Foundation of China (NSFC Nos. 51372195, 11574244, and 51402196), the CSS project (Grant No. YK2015-0602006), the Fundamental Research Funds for the Central Universities (2013JJDGZ03), Program for Innovative Research Team in the University of Ministry of Education of China (IRT13034), and the China Postdoctoral Science Foundation (Grant Nos. 2014M552229 and 2015T80915). X. J. Lou would like to thank the “One Thousand Youth Talents” program for support.

<sup>1</sup>J. F. Scott, *Ferroelectric Memories* (Springer, 2000).

<sup>2</sup>T. Choi, S. Lee, Y. Choi, V. Kiryukhin, and S.-W. Cheong, *Science* **324**, 63 (2009).

<sup>3</sup>S. Yang, J. Seidel, S. Byrnes, P. Shafer, C.-H. Yang, M. Rossell, P. Yu, Y.-H. Chu, J. Scott, and J. Ager, *Nat. Nanotechnol.* **5**, 143 (2010).

<sup>4</sup>R. Nechache, C. Harnagea, S. Li, L. Cardenas, W. Huang, J. Chakrabarty, and F. Rosei, *Nat. Photonics* **9**, 61 (2015).

<sup>5</sup>I. Grinberg, D. V. West, M. Torres, G. Gou, D. M. Stein, L. Wu, G. Chen, E. M. Gallo, A. R. Akbashev, and P. K. Davies, *Nature* **503**, 509 (2013).

<sup>6</sup>B. H. Park, B. S. Kang, S. D. Bu, T. W. Noh, J. Lee, and W. Jo, *Nature* **401**, 682 (1999).

<sup>7</sup>J. F. Scott and M. Dawber, *Appl. Phys. Lett.* **76**, 3801 (2000).

<sup>8</sup>M. Dawber and J. F. Scott, *Appl. Phys. Lett.* **76**, 1060 (2000).

<sup>9</sup>E. L. Colla, D. V. Taylor, A. K. Tagantsev, and N. Setter, *Appl. Phys. Lett.* **72**, 2478 (1998).

<sup>10</sup>Q. Jiang, W. Cao, and C. L. Eric, *J. Am. Ceram. Soc.* **77**, 211 (1994).

<sup>11</sup>A. M. Bratkovsky and A. P. Levanyuk, *Phys. Rev. Lett.* **84**, 3177 (2000).

<sup>12</sup>X. J. Lou, M. Zhang, S. A. Redfern, and J. F. Scott, *Phys. Rev. Lett.* **97**, 177601 (2006).

<sup>13</sup>X. J. Lou, M. Zhang, S. A. T. Redfern, and J. F. Scott, *Phys. Rev. B* **75**, 2288 (2007).

<sup>14</sup>K. Amanuma, T. Hase, and Y. Miyasaka, *Jpn. J. Appl. Phys.* **33**, 5211 (1994).

<sup>15</sup>W. Warren, B. Tuttle, and D. Dimos, *Appl. Phys. Lett.* **67**, 1426 (1995).

<sup>16</sup>X. Lou, *J. Appl. Phys.* **105**, 024101 (2009).

<sup>17</sup>J. Nuffer, D. C. Lupascu, and J. Rödel, *Appl. Phys. Lett.* **80**, 1049 (2002).

<sup>18</sup>H. Huang, *Nat. Photonics* **4**, 134 (2010).

<sup>19</sup>F. Liu, W. Wang, L. Wang, and G. Yang, *Appl. Phys. Lett.* **104**, 103907 (2014).

<sup>20</sup>D. Cao, J. Xu, L. Fang, W. Dong, F. Zheng, and M. Shen, *Appl. Phys. Lett.* **96**, 192101 (2010).

<sup>21</sup>A. Mischenko, Q. Zhang, J. Scott, R. Whatmore, and N. Mathur, *Science* **311**, 1270 (2006).

<sup>22</sup>D. Cao, C. Wang, F. Zheng, W. Dong, F. Liang, and M. Shen, *Nano Lett.* **12**, 2803 (2012).

<sup>23</sup>P. Zhang, D. Cao, C. Wang, M. Shen, X. Su, L. Fang, W. Dong, and F. Zheng, *Mater. Chem. Phys.* **135**, 304 (2012).

<sup>24</sup>F. Zheng, Y. Xin, W. Huang, J. Zhang, X. Wang, M. Shen, W. Dong, L. Fang, Y. Bai, and X. Shen, *J. Mater. Chem. A* **2**, 1363 (2014).

<sup>25</sup>H. Yi, T. Choi, S. Choi, Y. S. Oh, and S. W. Cheong, *Adv. Mater.* **23**, 3403 (2011).

<sup>26</sup>S. Yang, L. Martin, S. Byrnes, T. Conry, S. Basu, D. Paran, L. Reichertz, J. Ihlefeld, C. Adamo, and A. Melville, *Appl. Phys. Lett.* **95**, 062909 (2009).

<sup>27</sup>L. Pintilie, I. Vrejoiu, D. Hesse, G. Lerhun, and M. Alexe, *Phys. Rev. B* **75**, 512 (2007).

<sup>28</sup>M. Qin, K. Yao, Y. C. Liang, and B. K. Gan, *Appl. Phys. Lett.* **91**, 092904 (2007).

<sup>29</sup>A. Kholkin, O. Boiarkine, and N. Setter, *Appl. Phys. Lett.* **72**, 130 (1998).

<sup>30</sup>Y. S. Yang, S. J. Lee, S. Yi, B. G. Chae, S. H. Lee, H. J. Joo, and M. S. Jang, *Appl. Phys. Lett.* **76**, 774 (2000).

<sup>31</sup>M. Qin, K. Yao, Y. C. Liang, and S. Shannigrahi, *J. Appl. Phys.* **101**, 014104 (2007).

<sup>32</sup>M. Qin, K. Yao, and Y. C. Liang, *J. Appl. Phys.* **105**, 061624 (2009).

<sup>33</sup>D. Cao, H. Zhang, L. Fang, W. Dong, and F. Zheng, *Appl. Phys. Lett.* **97**, 102104 (2010).

<sup>34</sup>J. Xu, D. Cao, L. Fang, F. Zheng, M. Shen, and X. Wu, *J. Appl. Phys.* **106**, 113705 (2009).

<sup>35</sup>D. A. Hall and M. M. Ben-Omran, *J. Phys.: Condens Matter* **10**, 9129 (1998).

<sup>36</sup>Z. Luo, X. Lou, F. Zhang, Y. Liu, D. Chang, C. Liu, Q. Liu, B. Dkhil, M. Zhang, and X. Ren, *Appl. Phys. Lett.* **104**, 142904 (2014).

<sup>37</sup>T. Rojac, H. Ursic, A. Bencan, B. Malic, and D. Damjanovic, *Adv. Funct. Mater.* **25**, 2099 (2015).